Engineered Science
DOI: https://dx.doi.org/10.30919/es1096

Forecasting the Ultimate Strength of Designed Thin-Walled Very Large Crude Carrier Class Structures Based on Imperfection and Pressure Severities: Benchmarking and Developing an Empirical Formula

Aulia Widsay Salsabila Nisa,[1] Ristiyanto Adiputra,[2,*] Aditya Rio Prabowo,[1,*] Do Kyun Kim,[3] Heru Sukanto,[1] Yogie Muhammad Lutfi[1,4] and Muhammad Hanif Imaduddin[1,4]

Abstract

The increasing number of accidents involving very large crude carriers (VLCCs) has heightened concerns regarding ship safety and structural integrity. Stiffened panels have emerged as a crucial element in effectively reinforcing ship structures without significantly adding weight. Reliability analysis has been extensively conducted to evaluate the strength of stiffened panels with various parameters. However, the effects of lateral pressure parameters on structural strength have not received adequate attention in reliability analyses, and they have only been presented as single values. This necessitates a more extensive investigation to determine the distributional effects of lateral pressure on initial deflection enhancement and ultimate strength value reduction. To address this gap, the current study introduced modifications to parameters such as the slenderness ratio, span/bay ratio, yield strength, initial imperfections, and pressure. A total of 216 data points were obtained through numerical finite element method (FEM) simulations using ABAQUS. The obtained ultimate strength values were statistically analyzed using a T-test to explore the correlations among the parameters. Subsequently, a regression analysis was conducted to construct an empirical formula. The resulting empirical formula demonstrated remarkable accuracy, with a mean absolute percentage error (MAPE) of merely 0.801% when compared to the FEM numerical results, thus substantiating its validity as an effective and efficient solution for predicting ultimate strength values influenced by pressure.

Keywords: Stiffened panel; Ultimate strength; FEM; Pressure; Nonlinear regression; Empirical formula.
Received: 21 September 2023; Revised: 27 December 2023; Accepted: 03 January 2024.
Article type: Research article.

1. Introduction

Safety is a priority in the marine and offshore industries because they present a fairly high risk for humans, the marine environment, and transportation commodities. Oil tankers may require stronger safety criteria to avoid accidents such as oil spills and others. Three hundred and seventy-eight marine accidents occurred on oil tankers from 1998 to 2010.[1] Oil tankers often experience collisions, foundering/shipwrecks, fires/explosions, problems with ship structures, and oil leaks. Seven oil spills from oil tankers occurred in 2022, with four incidents releasing oil volumes of less than 700 metric tons. In addition, as noted in the Oil Tanker Spill Statistics[2] for 2022, there were large spills (>700 tons) in Asia and Africa and four medium spills (7-700 tons) in North America, Asia, and Africa. Oil tanker accidents caused by structural failures have happened in Hong Kong waters.[3] A total of 2012 marine accidents with 94 deaths were reported in Hong Kong waters in 2001–2005. According to the statistics,[4] crude oil tanker accidents involving the International Association of Classification Societies (IACS)[5] account for 97.76% of the total, with 97.35% of the deaths.

Based on these reports, it is necessary to evaluate the ultimate strength of stiffened panels, a crucial element of ship structures, to ensure their safety. A stiffened panel, consisting

[1] *Department of Mechanical Engineering, Universitas Sebelas Maret, Surakarta 57126, Indonesia.*
[2] *Research Center for Hydrodynamics Technology, National Research and Innovation Agency (BRIN), Surabaya 60112, Indonesia.*

of a longitudinal or transverse stiffener with a plate, improves the ship's strength-to-weight ratio and is one of the main construction elements on ship hull girders preventing sagging and hogging. The main geometric parameter affecting the ultimate strength value of stiffened panels is the plate and column slenderness.[6] Moreover, the combined load of longitudinal compression and lateral pressure decreases the ultimate strength due to increased initial deflection.[7,8] In line with this, the effect of lateral pressure on the ultimate strength of stiffened plates with combination loads was studied by Ma and Wang[9] to determine the change in the *pre-buckling strength* and initial deflection value. Another researcher analyzed lateral pressure and initial deformation effects using the Smith method and the nonlinear finite element method (NLFEM) to explain the critical factor.[10] Furthermore, Jiang and Zhang[11,12] predicted that a water height of 30 m, which corresponds to a lateral pressure of 0.3 MPa, would result in a 20% reduction in the HGUS value with symmetrical boundary conditions and an attached stiffened plate thickness of 18.5 mm. Similar research was conducted by Xu *et al*.[13], who found that the behavior of ship collapse was primarily influenced by increased lateral pressure. This is because the bending moment carried by the normal load increases the yielding, thereby reducing the ultimate strength. Additionally, the influence of the ultimate strength on the stiffened panels also depends on the span/bay ratio.[14] Sultana *et al*.[15] investigated the ultimate compressive strength of steel plates and stiffened panels based on several variables, such as the corrosion severity, span/bay ratio, and slenderness ratio. The ultimate strength of the stiffened panel was found to decrease linearly as the span/bay ratio increased.

The finite element method (FEM) is a numerical analysis method used to determine the approximate solutions to these problems. It is often used in solving engineering problems, such as obtaining the ultimate strengths of ship structures to improve their safety. The finite element method has been used to analyze structural strength,[6] which is a complicated process because it can predict the failure behavior of stiffened and unstiffened panels in detail. The FEM approach has been used to study a variety of ship types, including oil tankers,[16,17] bulk carriers,[18] and VLCC models.[18] The accuracy of the FEM simulation results depends on the complexity of the analysis, which includes the specified mesh density.[19] In the FEM meshing scheme, the general criterion used is that there is an even number of discrete elements, while the size of characteristic elements is in the range of (50,100) millimeters.[20] In addition, another factor that affects the accuracy of FEM results is the provision of boundary conditions (BCs). For plate and stiffened panels, the effects of BCs have been extensively studied.[21,22] For pessimistic (or robust) design, a simply supported boundary condition is typically used since it can provide structural designers with extra safety margins. The FEM approach divides the model into smaller components to examine the stiffened panel strength of each kind of ship. In the case of a stiffened panel structure, using a two-bay/two-span model is commonly recommended to account for the boundary effect area between adjacent spans.[23] As seen in Fig. 1, limit conditions on stiffened panels were determined by Li *et al*.[20] In Fig. 1, longitudinal girders and transverse frames are modeled by limiting out-of-plane movement and applying symmetrical boundary conditions to all four sides. This is applied in the FEM approach to handle the large number of variations that are typically evaluated and to save time during testing.

The geometry of the plate and stiffeners affects the stiffened panel's ultimate strength behavior. The typical geometry of a stiffened panel, as illustrated in Fig. 2, is commonly used in ships and ship-shaped offshore structures. The panel is composed of a stiffener and plate in longitudinal and transverse directions.[24]

In analyzing the ship's structure, structural imperfection factors must also be considered. In general, stiffened panels have geometric errors in the form of initial imperfections resulting from the measurement or manufacturing process, which provide a mechanism for nonlinear behavior synchronized with compressive loads.[25] The material, thickness, corrosion degradation, and corrosion level affect the existence of the initial geometric imperfections.[9] Research on the strength of stiffened panels under axial compression with the application of initial geometric imperfection effects through the FEM was carried out by Shi *et al*.[26] They found that initial geometric imperfections have a significant influence on the ultimate strength. Improper assumptions regarding the initial imperfections in the stiffened plate lead to an overestimation of the ultimate strength by 22% to 38%. Furthermore, several studies have researched the effect of geometric imperfections in stiffened panels in the buckling mode on their ultimate strength. Li *et al*.[27] performed a numerical investigation on the ultimate strength of stiffened panels subjected to uniaxial compressive load with imperfections in the form of initial deformation and buckling

[3] *Department of Naval Architecture and Ocean Engineering, Seoul National University, Seoul 08826, South Korea.*
[4] *Laboratory of Design and Computational Mechanics, Faculty of Engineering, Universitas Sebelas Maret, Surakarta 57126, Indonesia.*
**Email:* ristiyanto.adiputra@brin.go.id (R. Adiputra); aditya@ft.uns.ac.id (A.R. Prabowo)

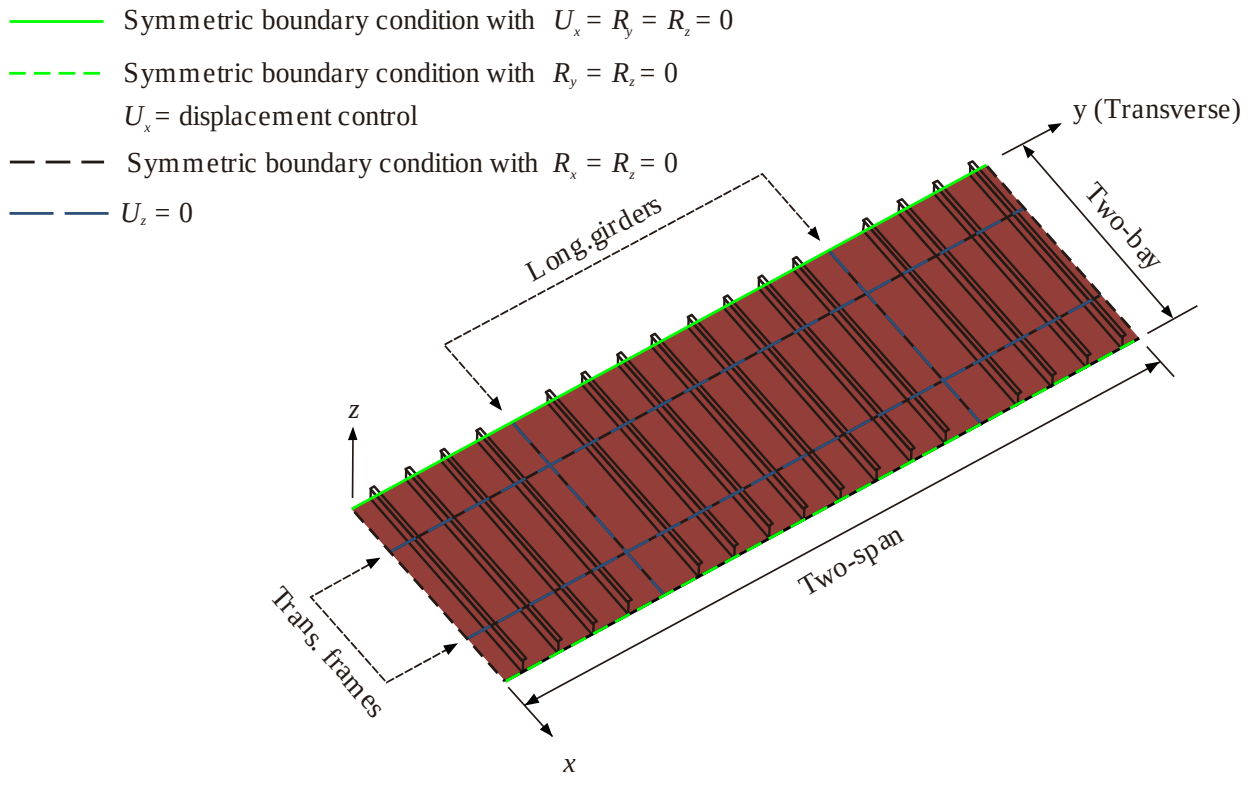

Fig. 1 The applied boundary conditions of the FE model for a stiffened panel. The figure was designed based on a reference. Reproduced with permission from [20], copyright 2022, the authors.

modes. They discovered that overall buckling modes have a considerable impact (either positive or negative) on the ultimate strength. Shi *et al*.[26] also investigated the effect of initial geometric imperfections with a higher buckling mode. In addition, according to the analytical findings of Estefen *et al*.,[28] imperfections in the local buckling mode have the largest impact on decreasing ultimate strength under axial compression conditions. The larger the initial geometric imperfection is, the smaller the ultimate strength.[29]

This research investigated the ultimate strength of designed thin-walled VLCC class structures under the integrated effects of imperfection and pressure severities, a relatively new area that has not been extensively studied. Prior research may have focused on an individual aspect. However, this study recognizes the interconnectedness of imperfections and pressure loads, providing a more holistic understanding of their combined impact on structural integrity. Previous studies have found that pressure causes a decrease in the strength of ship structures. However, these studies did not apply pressure value variations, so the distribution trend is not known. Therefore, it is essential to modify and vary the pressure so that the distribution trend and its effect on stiffened panels can be elucidated. To determine the trend and distribution effect of pressure on the strength of the ship structure, this study assumed variations in pressure with values of 0.04, 0.08, 0.12, and 0.16 MPa and other stiffened panel parameters. Three types of models were distinguished based on geometric aspects in the form of the slenderness ratio (plate, web, and column slenderness ratio), three variations of span values, three variations of initial imperfection amplitude values, two variations of yield strength, and four variations of pressure values cross-combined to obtain 216 ultimate strength data. The analysis was carried out by applying pressure in the first step and imposed displacement in the second step. Both steps were run on ABAQUS software. The relationship and correlation of each parameter with the ultimate strength value were analyzed to devise an empirical formula using the regression method. Empirical formulas in the functions of the slenderness ratio (plate, web, and column slenderness ratio), span/bay ratio, initial imperfection, and pressure were proposed and validated, predicting accurate ultimate strength values. Unlike previous studies that relied solely on theoretical models for the prediction of ultimate strength, this study emphasized introducing a comprehensive empirical model that surpasses simplistic approaches. It considered the complex interplay between imperfections and pressure severities, providing a more accurate representation of the actual behavior of thin-walled VLCC structures.

2 Methodology

2.1 Research Guideline

The analysis guideline for predicting the ultimate strength

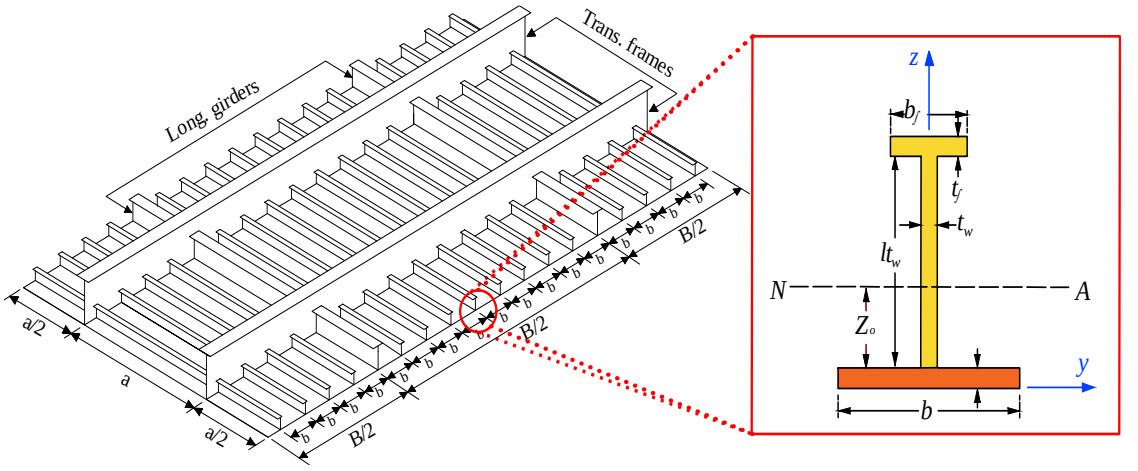

Fig. 2 Schematic view of the stiffened panel geometry in ships and ship-shaped offshore structures. The figure was designed based on a reference. Reproduced with permission from [22].

value is presented in Fig. 3. The selected model was determined based on geometric parameters, namely, the slenderness ratio and span/bay ratio. After that, each model was again varied based on the yield strength value and the influence of initial imperfections and pressure. The model was designed and analyzed using ABAQUS NLFEM simulation code by configuring the model range ½ + ½ bay – ½ + ½ span. After inputting the material properties and boundary conditions, the model was given the influence of the initial imperfections through changing nodes. The first step of the simulation was carried out only by applying pressure, which was continued at the second step by giving forced displacement. The ultimate strength results were compared with IACS regulations to further process the 216 data generated. The regression method was chosen to produce an empirical formula that considers the slenderness ratio (plate, web, and column slenderness), span/bay ratio, initial imperfection, and pressure. Validation was accomplished via statistical data processing of the FE analysis results.

2.2 IACS-CSR

The International Association of Classification Societies–Common Structural Rules for Bulk Carriers (IACS-CSR), which was updated as the IACS Harmonised Common Structural Rules (CSR-H), was used to predict the ultimate strength of stiffened panels by assuming failures such as several buckling modes, including column buckling, torsional buckling, and local buckling. Then, the three results were compared, and the ultimate strength was calculated using the smallest value. The following Equations (1)-(3) are mathematical forms that predict the ultimate strength value assuming column, torsional, and local buckling modes based on the IACS-CSR.

The difference between the three buckling modes above is that the column buckling mode considers the response of the stiffened panel to the whole buckling based on the Euler beam theory. The torsional buckling mode considers the tripping load that acts on the stiffened panel, especially the web part. In contrast, the local buckling mode considers the partial collapse of the stiffened panel due to its disproportionate thickness.

$$\sigma_{CR\,1} = \phi\sigma_{C1}\frac{A_s+A_{pE}}{A_s+A_p} \tag{1}$$

$$\sigma_{CR2} = \phi\frac{A_s\sigma_{C2}+A_p\sigma_{CP}}{A_s+A_p} \tag{2}$$

$$\sigma_{CR3} = \phi\frac{10^3 b_E t_p R_{eHp}+(h_{we}t_w+b_f w_f)R_{eHs}}{10^3 b t_p+h_{we}t_w+w_f t_f} \tag{3}$$

2.3 Initial imperfections

For the initial imperfections used in the simulation, we referred to the buckling results of the stiffened panel model to obtain the ultimate strength. To determine the geometry and the magnitude of imperfections caused during the ship's manufacturing and production processes, the coordinates of all nodes were modified with three imperfection modes: column, torsional, and local imperfection modes.[30]

$$W_c = B_0 \sin\frac{\pi x_i}{a} \tag{4}$$

$$W_t = B_0\frac{z_i}{hs}\sin\frac{\pi x_i}{a} \tag{5}$$

$$W_l = C_0 \sin\frac{m\pi x_i}{a}\sin\frac{\pi y_i}{b} \tag{6}$$

Here,

$$B_0 = a/1000 \tag{7}$$

$$C_0 = 0.1\,\beta_p{}^2 t_p, \text{ which } \beta_p = \frac{b}{t_p}\sqrt{\frac{\sigma_Y}{E}} \tag{8}$$

The stiffened panel model was given imperfection amplitude variations of 50%, 75%, and 100% or, as written in the formula,

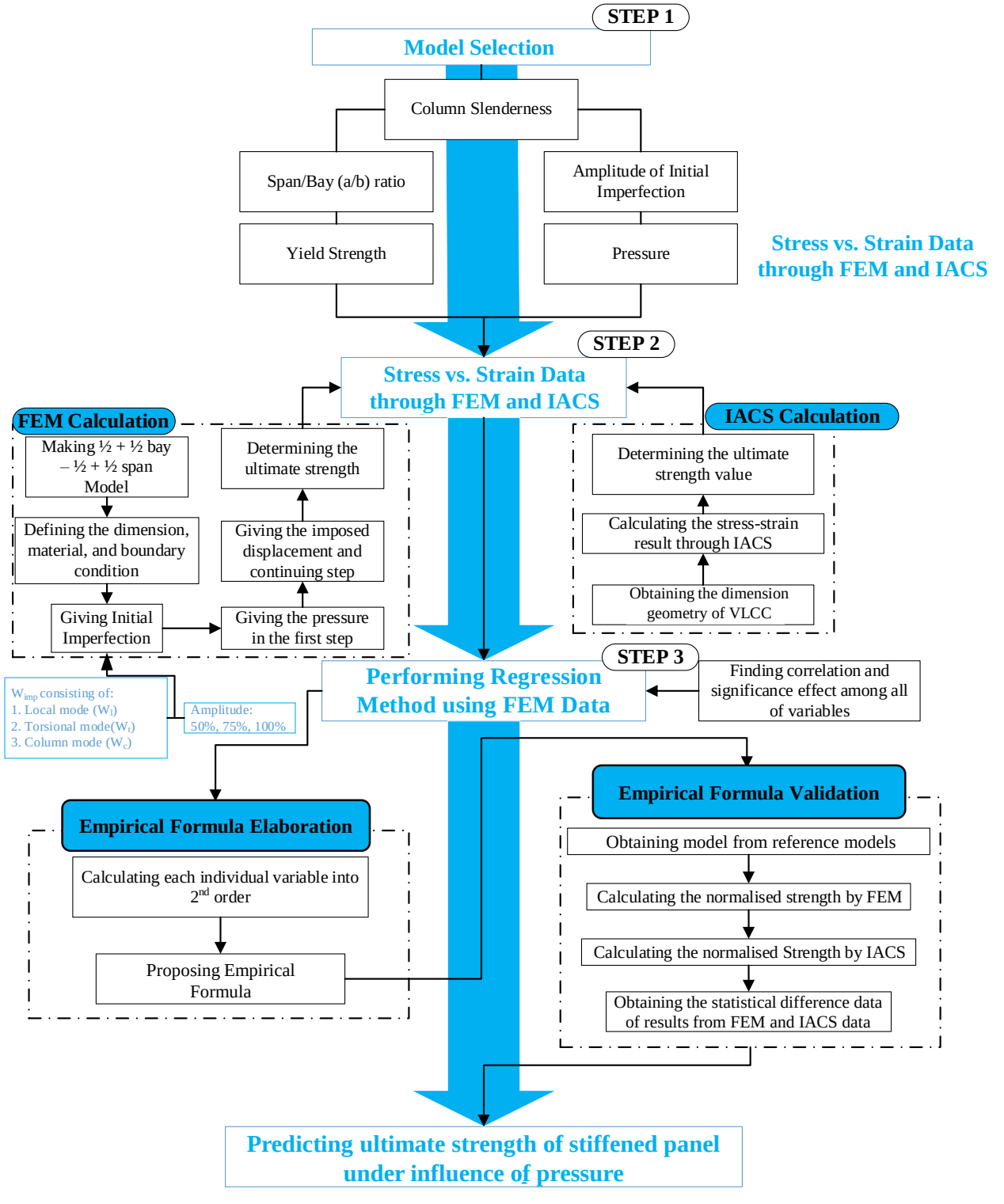

Fig. 3 Flowchart of model selection steps and analysis using the finite element method (FEM).

0.05, 0.075, and 0.1, respectively. In this study, the initial imperfections were provided by assigning a uniform amplitude value to the model. So, if one type of imperfection mode was given an amplitude value of 50% or 0.05, the other imperfection modes were also the same. In the present study, we set a 50-100% amplitude of the initial imperfections by specifying the imperfections directly as a table of node numbers and coordinate perturbations in the global coordinate system. The amplitude value of 0.05, 0.075, or 0.1 was considered as a constant value of B_0 and C_0, in which B_0 represents the magnitude of the initial geometric imperfection amplitude for column and torsional buckling and C_0 represents the initial geometric imperfection of local buckling. Then, we defined the parameter of B_0 in the column and the torsional

buckling mode formula, symbolized by W_c and W_t. The parameter of C_0 in the local buckling mode formula is represented by W_l. The amplitude value of initial geometric imperfections was determined by summing all imperfection modes from the reference formulation as shown in Equations (4)-(6). Therefore, in the following discussion, W_{imp} represents the three types of imperfection modes. When combined, the shape of the three imperfection modes is the node set to which the geometric imperfection values are to be applied in the global coordinate system, as seen in Fig. 4.

2.4 Case configuration

In this study, the type of ship used as a reference was an oil tanker (VLCC), which transports oil or similar products in large quantities. The stiffened panel on the hull, the part of the ship that is in direct contact with seawater pressure, was examined to determine the effect of pressure on the ultimate strength of the ship's structure. The VLCC oil tanker ship was referenced from ISSC-2000,[31] as seen in Fig. 5, which illustrates the cross-section of the VLCC. Based on the cross-section reference, the VLCC was found to have 48 models of stiffened panels of different sizes, types, and material properties, which are also defined in Tables 1 and 2.

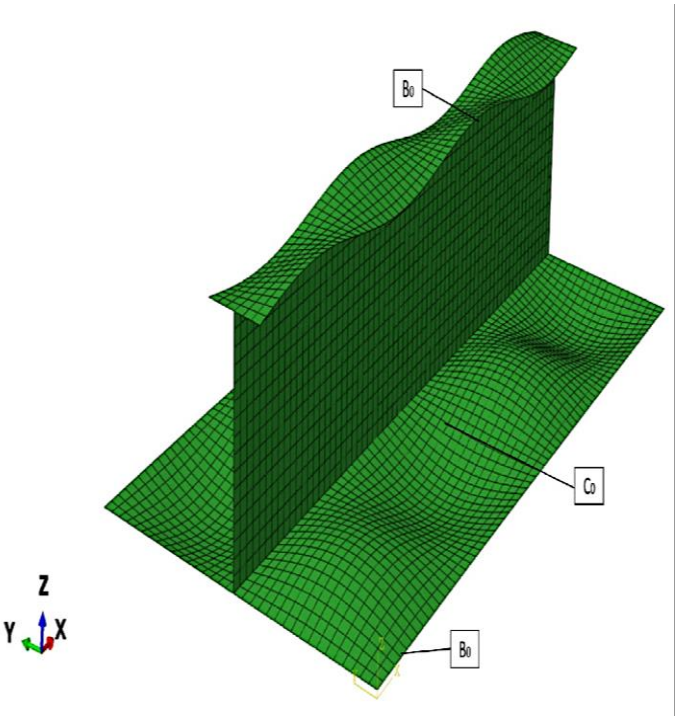

Fig. 4 The initial imperfection with three imperfection modes applied to the FE model in the global coordinate system.

Table 1. Dimensions of the stiffened panels on the double-hull VLCC.

No.	Dimensions	Type	Yield Stress (MPa)	No.	Dimensions	Type	Yield Stress (MPa)
1	300x90x13/17 IA	Angle-bar	313.6	25	250x90x12/16 IA	Angle-bar	313.6
2	350x100x12/17 IA	Angle-bar	313.6	26	450x11+150x22	Tee-bar*	325.8
3	400x100x11.5/17 IA	Angle-bar	313.6	27	450x11+150x19	Tee-bar*	352.8
4	400x11+150x12	Tee-bar*	313.6	28	450x11+150x16	Tee-bar*	352.8
5	400x11+150x14	Tee-bar*	313.6	29	450x11+150x14	Tee-bar*	352.8
6	450x11+150x12	Tee-bar*	313.6	30	450x11+150x12	Tee-bar*	352.8
7	450x11+150x14	Tee-bar*	313.6	31	450x11+150x14	Tee-bar*	325.8
8	450x11+150x16	Tee-bar*	313.6	32	400x100x11.5/16 IA	Angle-bar	352.8
9	450x11+150x19	Tee-bar*	313.6	33	350x100x12/17 IA	Angle-bar	352.8
10	450x11+150x22	Tee-bar*	313.6	34	300x90x13/17 IA	Angle-bar	352.8
11	450x11+150x25	Tee-bar*	313.6	35	850x17+150x19	L-bar*	352.8
12	500x11+150x28	Tee-bar*	313.6	36	250x90x12/16 IA	Angle-bar	325.8
13	500x11+150x30	Tee-bar*	313.6	37	300x90x12/16 IA	Angle-bar	352.8
14	500x11+150x32	Tee-bar*	313.6	38	400x11+150x14	Tee-bar*	352.8
15	500x11+150x34	Tee-bar*	313.6	39	450x11+150x12	Tee-bar*	352.8
16	550x12+150x30	Tee-bar*	313.6	40	450x11+150x14	Tee-bar*	352.8
17	550x12+150x25	Tee-bar*	313.6	41	450x11+150x16	Tee-bar*	325.8
18	350x100x12/17 IA	Angle-bar*	313.6	42	450x11+150x19	Tee-bar*	352.8
19	550x12.5+150x32	Tee-bar*	325.8	43	450x11+150x22	Tee-bar*	352.8
20	500x11.5+150x30	Tee-bar*	352.8	44	450x11+150x25	Tee-bar*	352.8
21	500x11.5+150x28	Tee-bar*	352.8	45	450x11+150x28	Tee-bar*	352.8
22	500x11+150x25	Tee-bar*	352.8	46	500x11+150x25	Tee-bar*	352.8
23	450x11+150x28	Tee-bar*	352.8	47	500x11+150x28	Tee-bar*	352.8
24	250x12.5	At-bar	313.6	48	230x12.5	At-bar	313.6

Table 2. Material properties of the stiffened panels on the double-hull VLCC.[31]

Properties [Units]	Value
Young's Modulus [MPa]	205,800
Poisson's Ratio	0.3
Yield stress [MPa]	313.6
Plastic Tangent Modulus	0

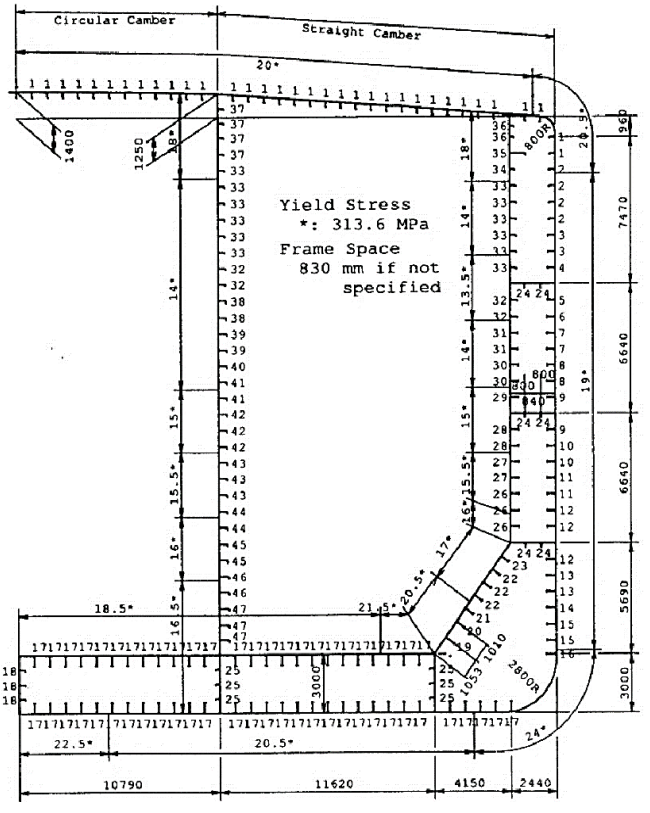

Fig. 5 Hull girder cross-section of a double-hull VLCC. Reproduced with permission from [31].

Notably, there are variations in the types of stiffened panel shapes in the double-hull VLCC. Stiffened panel models were selected from these 48 models for this research by collecting random data from several stiffened panel sizes. The data were plotted on a graph to obtain the distribution of stiffened panel data for the mid-ship section, as shown in Fig. 6. Fig. 6 contains a graph that compares several variables, such as the area of inertia, column slenderness, web slenderness, and plate slenderness. The column slenderness, plate slenderness, and web slenderness ratios are calculated using Eqs (9)-(10).

$$\lambda = \frac{a}{\pi r}\sqrt{\frac{\sigma_Y}{E}} \tag{9}$$

$$\beta_p = \frac{b}{t_p}\sqrt{\frac{\sigma_Y}{E}} \tag{10}$$

$$\beta_w = \frac{h_w}{t_w}\sqrt{\frac{\sigma_Y}{E}} \tag{11}$$

As shown in Fig. 6, the models were categorized into light, medium, and heavy based on the differences in their area of inertia, column slenderness, web slenderness, and plate slenderness. The difference was caused by the geometries of the stiffened panels in every model, such as their plate, web, and flange dimensions. In general, the light model has the smallest geometries, followed by the medium model, and the heavy model has the greatest geometries. According to the stiffened panel model selection in Fig. 6(a), the light stiffened panel model had the smallest area of inertia but a large column slenderness value. Conversely, the heavy model had a large area of inertia but the smallest column slenderness value. The area of inertia and column slenderness of the medium model had values in the middle.

In comparisons of the area of inertia and the value of plate slenderness in Fig. 6(b), the light model had the smallest area of inertia, followed by the medium model in the middle and then the heavy model with the largest area of inertia. When viewed based on the value of plate slenderness, the heavy

Table 3. The dimensions of each stiffened panel model.

Model	w_p (mm)	Span (mm)	t_p (mm)	h_w (mm)	t_w (mm)	w_f (mm)	t_f (mm)
Light Model	830	830	14	400	11	150	12
		1660					
		2490					
Medium Model	830	830	17	450	12	150	22
		1660					
		2490					
Heavy Model	830	830	20	550	13	150	32
		1660					
		2490					

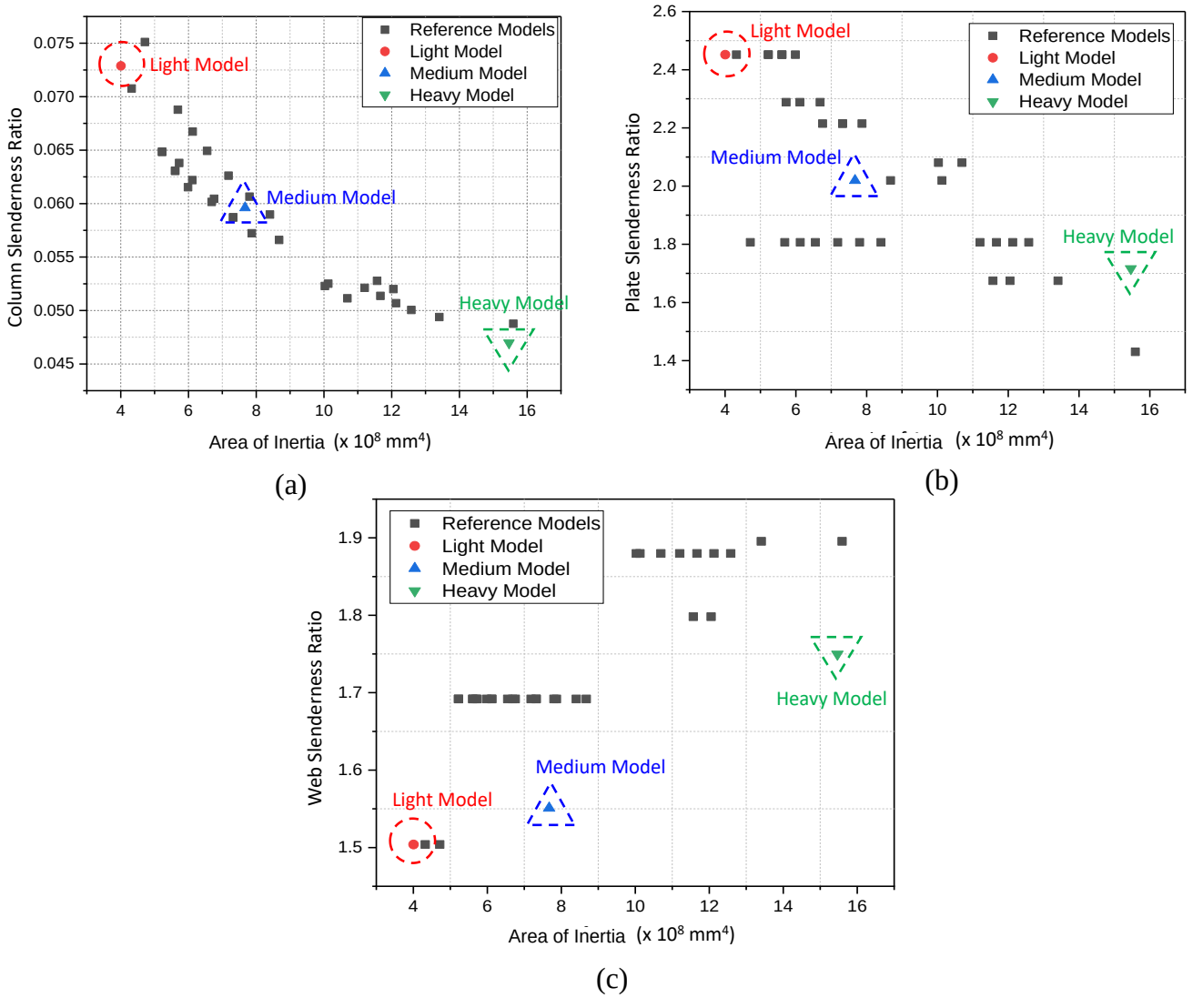

Fig. 6 Comparison of the area of inertia with geometric parameters: (a) column slenderness, (b) plate slenderness, and (c) web slenderness.

model had the most significant value, the light model had the smallest value, and the medium model fell between the two. These data demonstrate that the relationship between the area of inertia and the value of plate slenderness was directly proportional. In Fig. 6(c), the area of inertia in the light model was the smallest, and its value of web slenderness was the lowest. This indicated a directly proportional relationship between the area of inertia and the value of the web slenderness.

Based on these three graphs, the stiffened panel data at the bottom, middle, and top were designated as stiffener numbers 4, 19, and 45 for the light, medium, and heavy models, respectively, to represent the values of the entire stiffened panel model that was under pressure due to seawater. The geometric dimensions of the selected models can be seen in Table 3, and the case configuration is examined in Table 4.

Table 4. Case configuration of the analyzed stiffened panel.

Model	Span/bay (a/b) ratio	Amplitude of Initial Imperfection (%)	Pressure (MPa)	σ_Y (MPa)
Light, Medium, and Heavy Model	1	50	0.04	313.6
	2	75	0.08	
			0.12	352
	3	100	0.16	

The three stiffened panel models were subjected to several parameter variations as case configurations in this study, including as many as three variations of the span/bay ratio, with large yield strength of 313.6 and 352 MPa and variations of the initial imperfection amplitude of 50%, 75%, and 100%. The stiffened panel began with normal pressure conditions that

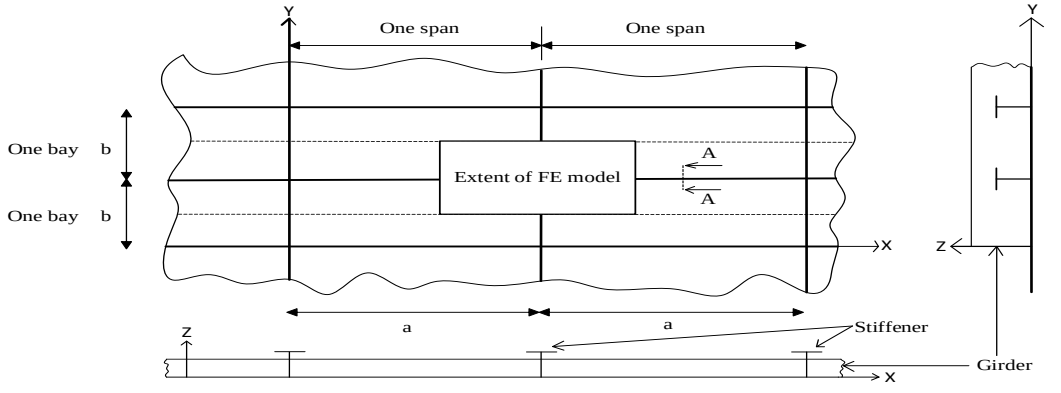

Fig. 7 The extent of the selected cross-sectional geometry of the stiffened panel models for FEM analysis.

increased to extreme conditions, namely, 0.04, 0.08, 0.12, and 0.16 MPa. From the case configuration above, it can be seen that the scenario cases that were considered in this study by cross-combining each variation totaled as many as 216 cases.

2.5 Finite element modeling

The finite element method was carried out using ABAQUS software to analyze the ultimate strength of the stiffened panels. The representative geometry of a stiffened panel was its cross-sectional shape, consisting of 1/2 + 1/2 span and 1/2 + 1/2 bay, as shown in Fig. 7. An illustration of the stiffened panel model is shown in Fig. 8, which illustrates the width and thickness of the flange, the height and thickness of the web, and the width and thickness of the plate.

The boundary conditions for the stiffened panel model can be seen in Fig. 9, where the longitudinal and transverse edges are arranged equally for uniformity so that continuous conditions can be applied to the stiffened panel. In the simulation, transverse stiffeners were not modeled geometrically but only given boundary conditions as fixed constraints to simplify the calculations and modeling.

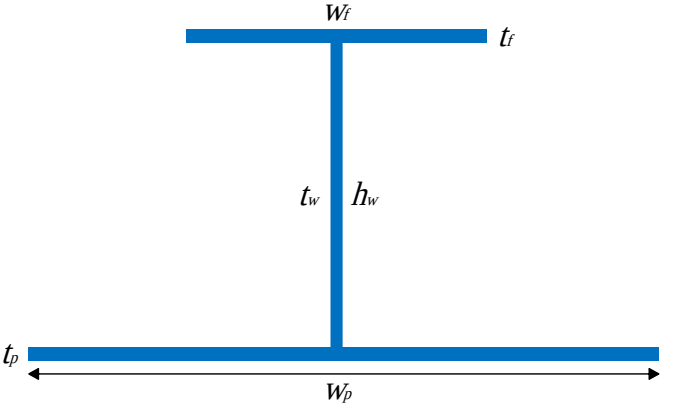

Fig. 8 Cross-sectional geometry of the stiffened panels.

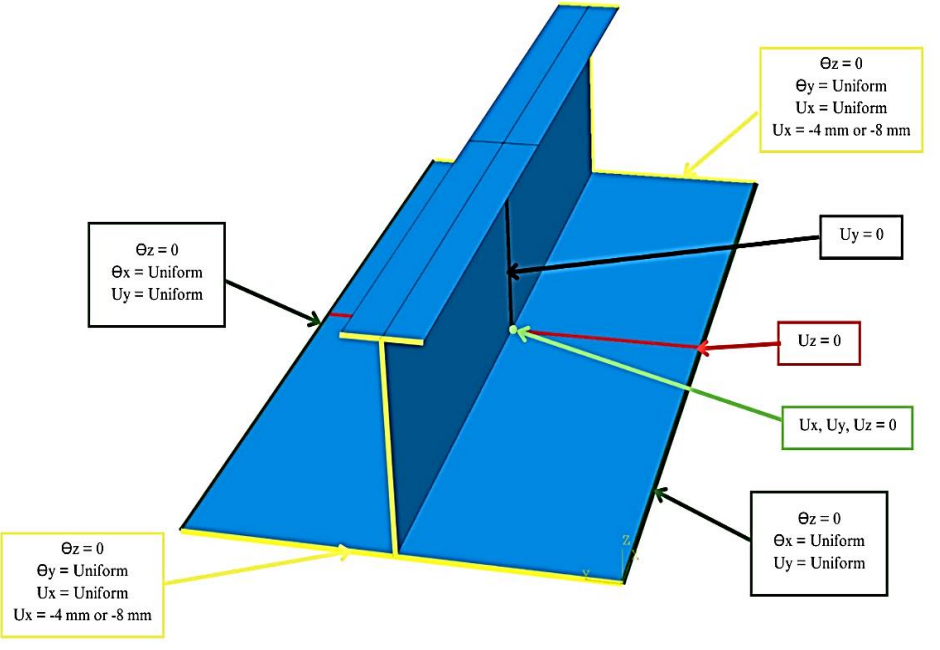

Fig. 9 Determined boundary conditions for the FEM analysis of the FE model.

Stiffened panels must be discretized through several elements to achieve convergence; therefore, to determine the appropriate mesh size in the modeling, a study of mesh convergence, as shown in Fig. 10, was conducted. Convergence was observed at a mesh size of 25 mm, so in the simulation, meshing was carried out with elements of length 25 mm, as shown in Fig. 11.

In applying the load on the stiffened panel model structure in the ABAQUS simulation,[32-36] the pressure was given under normal conditions to extreme conditions, namely, 0.04, 0.08, 0.12, and 0.16 MPa. Pressure was applied as a loading of the stiffened panel structure in the lateral and transverse directions given to the bottom of the plate and the sides of the stiffener.[37] Then, a load in the form of axial compression was given, which caused an imposed displacement of 5 mm in the direction of the axial stiffened panel. Details of the application of pressure and axial compression loads on the stiffened panel model structure can be seen in Fig. 12.

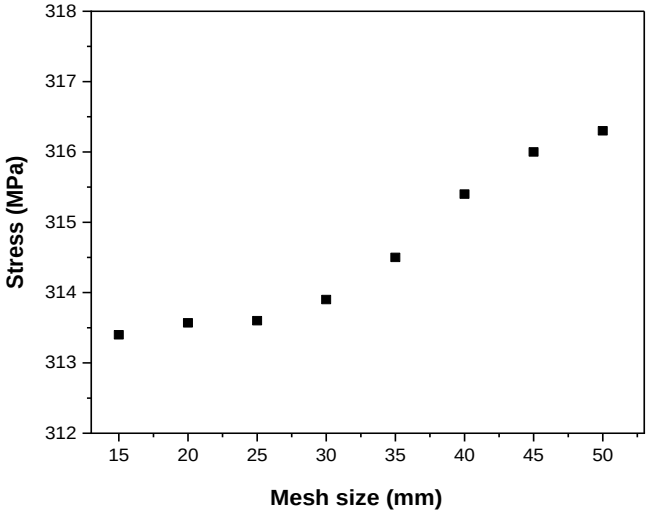

Fig. 10 Mesh convergence graph: meshes of size 15 and 50 mm.

3. Results and discussion

An analysis of the ultimate strength value calculation in the stiffened panel model was carried out using the FEM and IACS-CSR,[5] which was then evaluated to obtain the results. In this discussion, the results of the FEM and IACS-CSR[5,38-41] are compared. In addition, we consider the results of the FEM with no applied pressure. The variations in geometry, pressure, and yield strength parameters described earlier are compared with the results. From the 216 simulated data, only a few cases are shown so that explanations can be given effectively.

3.1 Geometry parameters

The following is a graph comparing the ultimate strength results from the FEM with and without pressure and results based on the IACS. It can be seen in Fig. 13 that the ultimate strength in all stiffened panel models with relative pressure was almost the same as that with no pressure. The small difference between the FEM and IACS results indicated that the results obtained with the FEM were appropriate. The graph shows an incomparable relationship between the increase in column slenderness and the ultimate strength. In addition, applying pressure to the stiffened panel also decreased the ultimate strength, even though it was a relatively small increase. Even so, from the resulting graph trend, the difference between the results with and without pressure increased when the column slenderness value was greater.

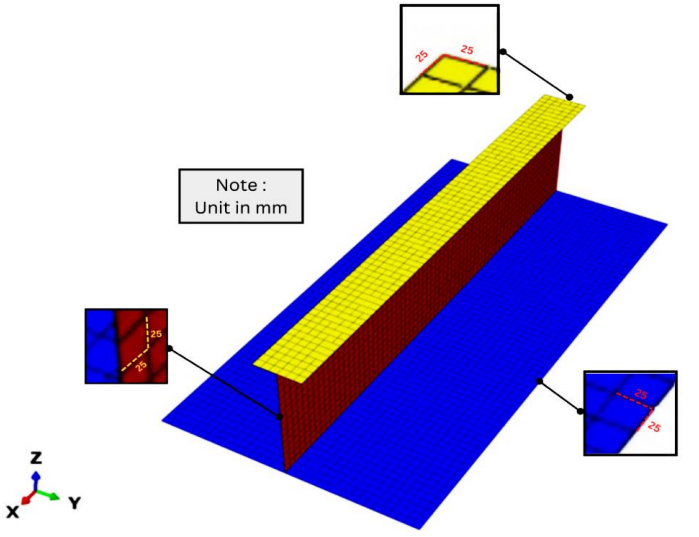

Fig. 11 Meshing configuration on the panel geometry of the model.

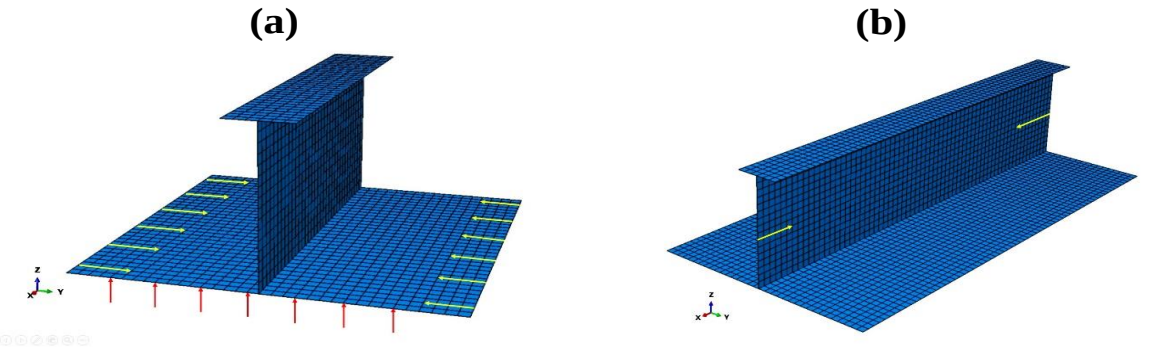

Fig. 12 Panel illustration of (a) applied load pressure on the FE model and (b) applied axial compression on the model.

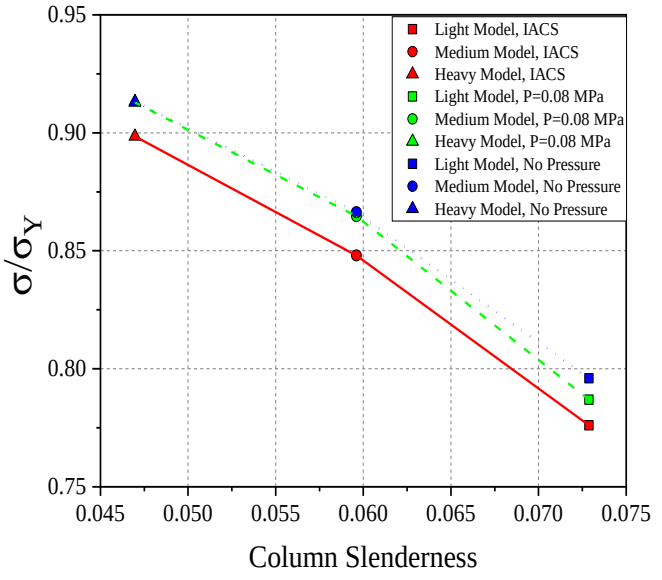

Fig. 13 Comparison graph of ultimate strength models with pressure effects based on the column slenderness.

Next, we performed a comparison by varying the span/bay ratio in the model. As shown in Fig. 14, the span/bay ratio had an inversely proportional relationship with the ultimate strength. In the case of span/bay ratio fluctuations, unlike for column slenderness, the bigger the span/bay ratio, the smaller the difference between the FEM findings with and without the application of pressure.

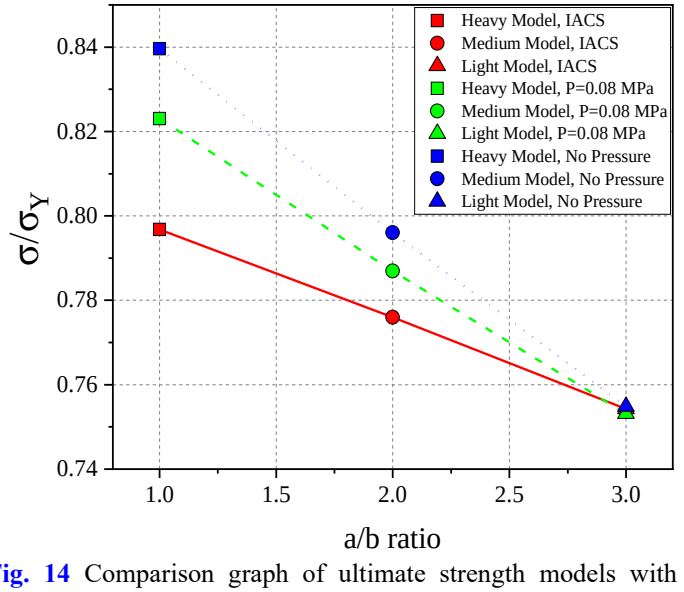

Fig. 14 Comparison graph of ultimate strength models with pressure effects based on the span/bay ratio.

3.2 Material properties

A comparison was made with two variations in yield strength values, *i.e.*, 313.6 and 352 MPa. Fig. 15 shows that the decrease in yield strength on the stiffened panel also caused a decrease in the ultimate strength. Thus, the yield strength was directly related to the ultimate strength. The comparison between pressured and non-pressured models showed a constant trend as the yield strength changed.

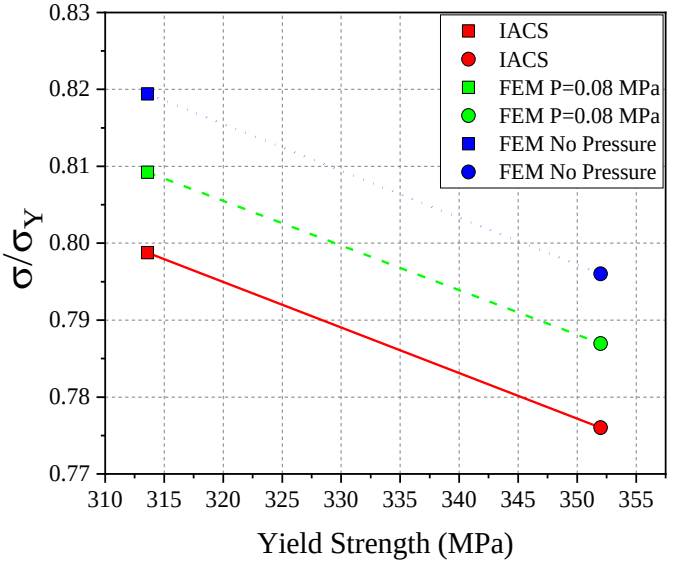

Fig. 15 Graph of the relationship between the yield strength and ultimate strength value results based on the IACS.

3.3 Lateral pressure

A comparison of the results with varying magnitudes of pressure applied to the model was also conducted, as shown in Fig. 16. Comparisons were made at pressure variations of 0, 0.04, 0.08, 0.12, and 0.16 MPa with the results from the IACS. In Fig. 16(a), the graph shows conformity with the values predicted by the IACS, with an insignificant difference. In Fig. 16(b), it can be seen that there was a downward trend with increasing pressure. The changes that occurred in the ultimate strength were nearly linear.

Von Mises contour illustrations are used to display the shape of deformation and stress affected by lateral pressure and the influence of initial imperfections. The graph in Fig. 17 represents a light-stiffened panel model. The other parameters used for the stiffened panel model were an initial imperfection amplitude value of 100%, span/bay ratio of 2, pressure of 0.08 MPa, and yield strength of 352 MPa. Four main points in the contour plot can be seen in Fig. 18, namely, the point when the panel was in the plastic region (A), when it reached the ultimate point (B), when it was in the post-buckling stage (C), and when it collapsed (D).

The middle and edges were noticeably subjected to great stress when the model was in the elastic region or region A. This was due to the application of pressure at the beginning of the calculation causing an initial deflection before the imposed displacement. When the ultimate point was reached, high levels of stress and displacement occurred on the plate. The

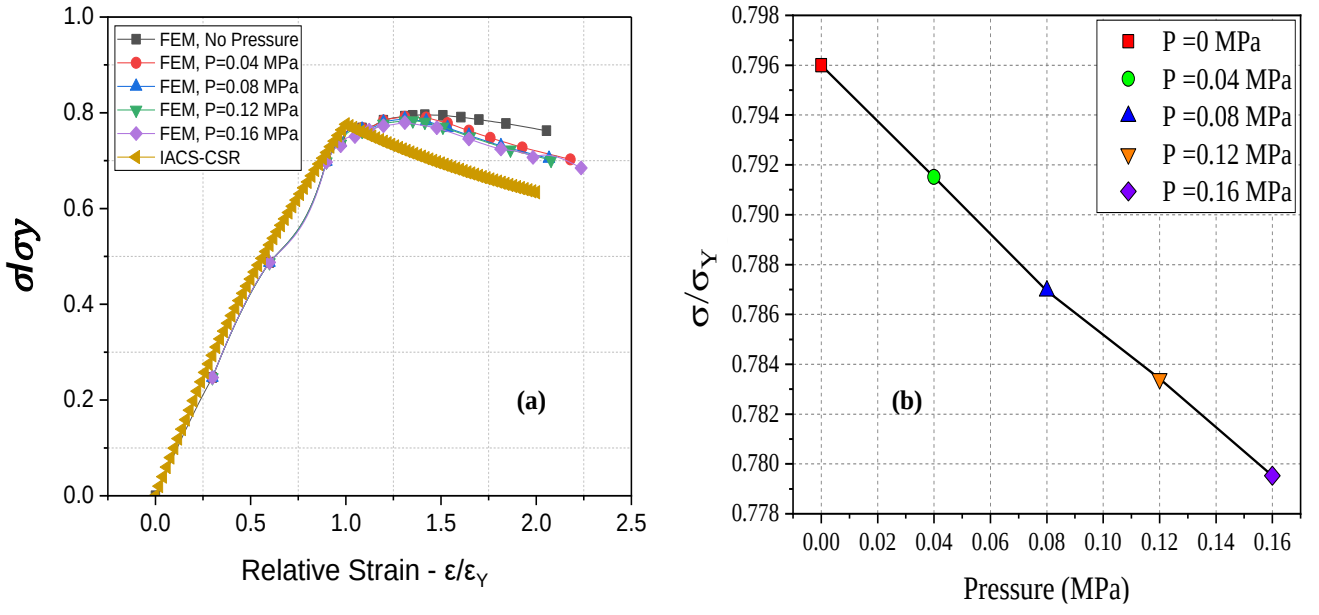

Fig. 16 Model graphs comparing the pressure variable and ultimate strength value.

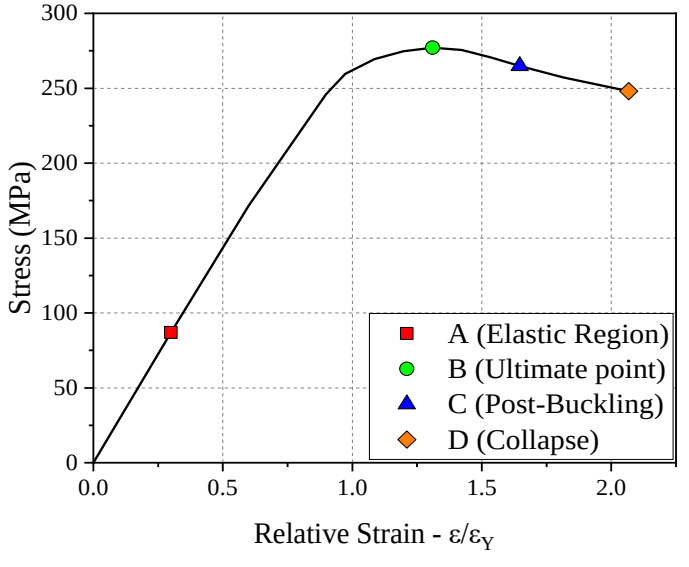

Fig. 17 Load-end shortening curve for the light model in the elastic region, at the ultimate point, in the post-buckling stage, and under collapse conditions.

provision of initial imperfections, one of which was a local imperfection mode, made the plate deformation even greater. In addition, the initial deflection due to the influence of pressure on the plate also increased the tension and deformation on the plate. Meanwhile, stress and deformation occurred evenly on the entire stiffened panel during post-buckling and collapse.

4. Formula elaboration

4.1 Correlation between ultimate strength and model variables

The comparisons of each parameter with the ultimate strength described in the previous section explained the effect exerted by each parameter. The relationship of each parameter with the ultimate strength value was subsequently processed statistically using the T-test, as shown in Table 5. All model parameters showed a level of significance that had a major effect on changes in the ultimate strength value. This can be seen where almost all parameters showed significance close to zero and T-values above the T-table. The negative values for some parameters indicated an inversely proportional relationship to the ultimate strength value. In this research, the values of initial imperfections, plate slenderness, and amount of pressure applied significantly affected the strength value of the stiffened panel.

Table 5. Correlation measurement for each model parameter using the T-test.

Parameter	T-value	Significance	T-Table	Significance Level
a/b	-0.383	0.702	± 1.971	0.05
W_{imp}	-41.022	<0.001		
P	-6.085	<0.001		
β_p	-23.090	<0.001		
β_w	-3.460	<0.001		
λ	-4.187	<0.001		

In addition to the statistical data, the correlation given to each model parameter is presented in graphic form in Fig. 19. Figs. 19(a) – (d) respectively show the inversely proportional effect of the model parameters span/bay ratio, initial imperfections, pressure, and plate slenderness on the normalized strength value. In Figs. 19(e) and (f), the graphs show fluctuating trends that do not clearly describe the

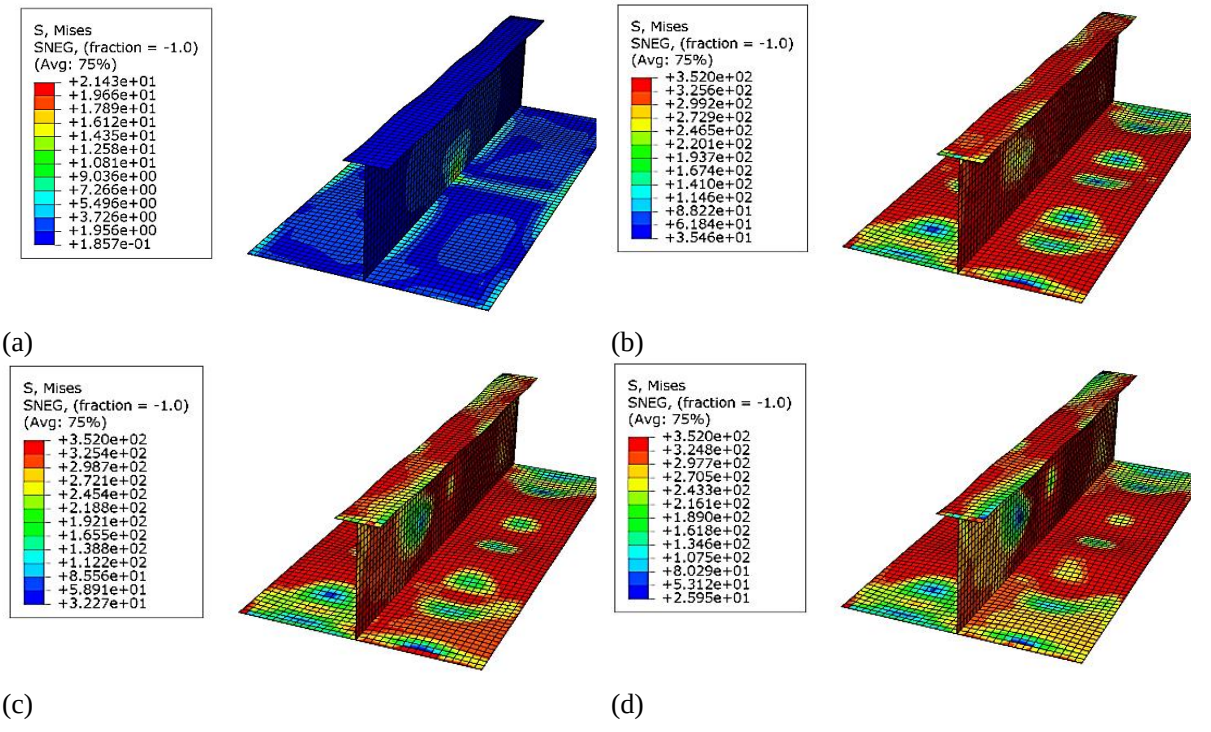

Fig. 18 The contour pattern of the light stiffened panel model under specific conditions: (a) plastic region, (b) ultimate point, (c) post-buckling, and (d) collapse.

relationships of column parameters and web slenderness with normalized strength. This is because both parameters were influenced and dominated by the effect of other model parameters. Thus, for both parameters, the relationship to the normalized strength value has a nonlinear form.

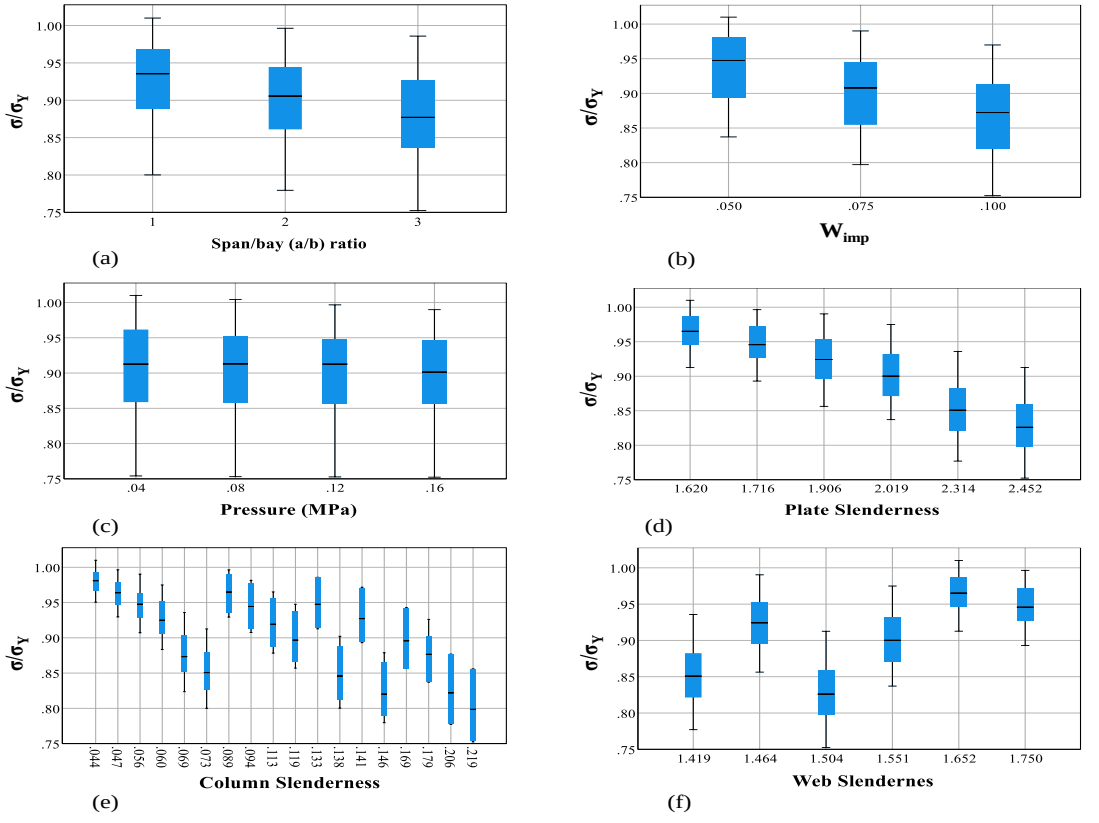

Fig. 19 Correlation measurement for each model parameter: (a) span/bay (a/b) ratio, (b) initial imperfections, (c) pressure, (d) plate slenderness, (e) column slenderness, and (f) web slenderness.

4.2 Empirical Formula for $\frac{\sigma_U}{\sigma_Y} = f(^{a}/_{b}, W_{imp}, P, \beta_p, \beta_w, \lambda)$

In this study, a formula was created to predict the ultimate strength value of the stiffened panel under the influence of the stiffened panel's geometric parameters (plate, web, column slenderness, and span/bay ratio), initial imperfections, and pressure, as described in Eq. (12).

$$\frac{\sigma_U}{\sigma_Y} = f(^{a}/_{b}, W_{imp}, P, \beta_p, \beta_w, \lambda) \quad (12)$$

Through regression analysis conducted using 216 numerical calculation (FEM) data, an empirical formula was developed to predict the ultimate strength value. This formula incorporated the influence of pressure, considering its significant effect on the strength of the stiffened panel. A quadratic formula model was chosen because it was able to describe the results with R^2 and adj. R^2 values of 0.972 and 0.970, respectively, represent a level of correctness predicted by the variable-parameter model of about 97% (see Table 6). In addition to showing the influence of the model parameters, empirical formulas in the form of quadratic equations also obtained accurate predictions and captured the nonlinear relationships between parameters.

The empirical formula can be written as follows:

$$\frac{\sigma_U}{\sigma_Y} = 1.457 - 0.005\,a/b - 1.457W_{imp} - 0.416\lambda - 0.153\beta_p - 0.053\beta_w - 0.489P^2 + 0.512\lambda^2\beta_w{}^2 - 0.746\lambda^2 \quad (13)$$

In the empirical formula, the pressure value hurts the increase in the ultimate strength value, as do the values of geometric parameters such as the plate and column slenderness and span/bay ratio. The inverse relationship of initial imperfections with the ultimate strength shown in the previous section also aligns with that given in the equation, where the coefficient value is negative.

4.3 Empirical Formula Validation for $\frac{\sigma_U}{\sigma_Y} = f(^{a}/_{b}, W_{imp}, P, \beta_p, \beta_w, \lambda)$

Validation of the empirical formula was performed by comparing the predicted ultimate strength results with the resulting values based on the FEM. Fig. 20 shows the comparison between the two, where the horizontal axis represents the empirical formula prediction, while the vertical axis shows the FEM simulation result. The graph shows that the results had reasonable accuracy, with a standard error between the two of only around 1.05%. Moreover, a statistical analysis in the form of mean absolute percentage error (MAPE) calculations was carried out to measure the error rate of the prediction results. A value of 0.801% indicated that the data produced by the empirical formula were accurate, and the equation formulated was appropriate for use. The current work may be extended to a comparison with the existing general empirical formula to observe the significance of pressure involvement in the proposed formula when calculating the ultimate strength.

Table 6. Result summary of regression to determine the empirical formula.

Constant	Unstandardized Variable								R^2	Adj. R^2
	a/b	W_{imp}	λ	β_p	β_w	P^2	$\beta_w{}^2\lambda^2$	λ^2		
1.457	-0.005	-1.457	-0.416	-0.153	-0.053	-0.489	0.512	-0.746	0.972	0.970

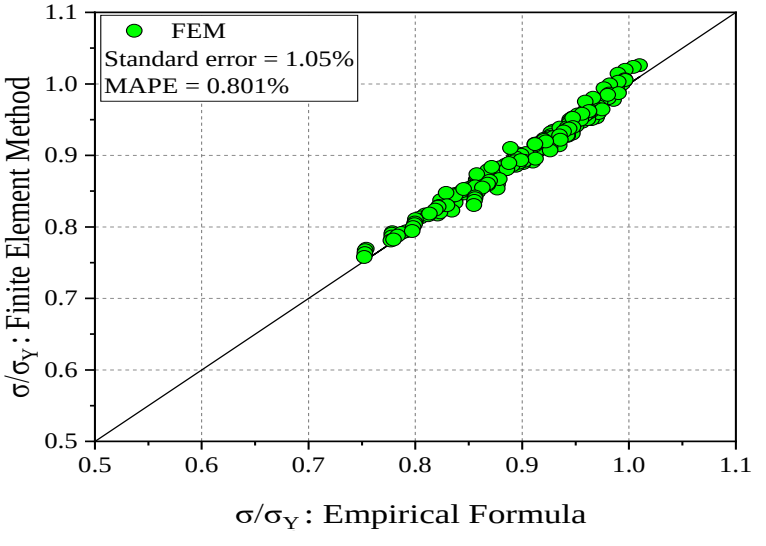

Fig. 20 Comparison of the empirical formula and the FEM results.

5. Conclusions

This study cross-combined data by varying several geometric parameters of stiffened panels that affected the panels' ultimate strength, such as the plate, web, and column slenderness and span/bay ratio, with other parameters, such as material properties in the form of yield strength and the influences of initial imperfections and pressure. The analysis was carried out through an FEM numerical calculation using ABAQUS software and a comparison with IACS regulations to create an empirical formula to predict the ultimate strength value.

- The modification of geometric parameters through variations in the slenderness ratio and span/bay ratio, as well as variations in the initial imperfections and pressure, significantly affected the ultimate strength value.
- The investigation produced an empirical formula that can accurately predict the ultimate strength value with an MAPE of 0.801%, and the quadratic equation in the empirical formula was able to represent the nonlinear relationships of each parameter.
- Empirical formulas obtained using regression methods can be an efficient and effective solution as compared to numerical and experimental methods when analyzing tee-bar-type stiffened panels due to the influence of pressure.
- The ultimate strength formula produced in this study can only be considered accurate for tee-bar-type stiffened panels.

Despite the valuable insights gained from this study, it is important to acknowledge several limitations. Firstly, the influence of pressure was considered only based on static load conditions. Secondly, the empirical formula was obtained from a portion of the geometry that was selected using FEM modeling; thus, limitations in the quantity or quality of data, especially for real-world VLCC structures, could impact the model's accuracy and generalizability. Thirdly, the formula can only be used on tee-bar-type stiffened panels, so caution should be exercised when extrapolating to different scenarios. These limitations relate to recommendations for further research, including extending the research by benchmarking the developed empirical model against experimental data from actual full-scale thin-walled VLCC structures. Comparing the model predictions with actual structural performance data under varying pressure severities will validate the model and enhance its applicability to practical scenarios. Additionally, further research is needed to validate the developed empirical model and assess its applicability to different structural configurations and materials beyond tee-bar-type stiffened panels. Future investigations must consider the effect of extreme loading conditions, such as dynamic loading conditions, on the ultimate strength of thin-walled VLCC structures. Examining the effects of variables such as dynamic pressure variations, loads caused by waves, and temporary environmental circumstances on the structural response is necessary to help researchers better understand the structural behavior.

Acknowledgments

This research was funded by the Indonesia Endowment Fund for Education Agency (LPDP) under the DAPT Equity Program of Universitas Sebelas Maret Year 2023/2024 with the assigned contract number 3272.1/UN27.22/PT.01.03/2023. This support is gratefully acknowledged by the authors.

Conflict of Interest

There are no conflicts of interest.

Supporting Information

Not applicable.

Nomenclature

Symbols/Name	Units	Description
A_s	cm^2	Net sectional area without attached plating
A_p	cm^2	Net sectional area of attached plating
a	mm	Span length
B_0	m	Amplitude for column and torsional imperfection mode
b, w_p	mm	Bay length
C_0	mm	Amplitude for local imperfection mode
E	N/mm^2	Young's Modulus
h_{we}	mm	Effective height of the web
h_w	mm	Web height of stiffener or primary supporting member
hs		Highest z coordinate of stiffened panel
m		Critical half-wave number at span
P	MPa	Pressure
R_{eHp}	MPa	Minimum yield stress of the material of the considered plate
R_{eHs}	MPa	Minimum yield stress of the material of the considered stiffener
r	mm	Radius of gyration
t_p	mm	Plate thickness
t_f	mm	Flange thickness
t_w	mm	Web thickness
U	mm	Initial displacement
u, x, y, z		Element coordinate
W_c	mm	Maximum value of the column imperfection mode
w_f	mm	Breadth of face plate or attached plating

W_{imp}	mm	Maximum value of the combined imperfection mode
W_l	mm	Maximum value of the local imperfection mode
W_t	mm	Maximum value of the torsional imperfection mode
β_{p}		Plate slenderness
β_w		Web slenderness
ε		Strain
ε_y		Yield strain
ε	MPa	Ultimate strength
λ		Column slenderness
$\sigma_{CR\,1}$	N	Column buckling mode
$\sigma_{CR\,2}$	N	Torsional buckling mode
$\sigma_{CR\,3}$	N	Local buckling mode
σ_{C1}	MPa	Critical stress
σ_{C2}	MPa	Critical stress
σ_Y	MPa	Yield strength
ϕ		Edge function

References

[1] U. Özkan, E. Başar, E. Köse, Risk Analysis of the Fire and Explosion Accidents in Oil Tankers, InMaritime Transport 2012 Conference 2012, 27-29.

[2] J. Chen, H. Chen, J. Shi, T. Yan, M. Gu, X. Huang, Factor diagnosis and governance strategies of ship oil spill accidents based on formal concept analysis, *Marine Pollution Bulletin*, 2023, **196**, 115606, doi: 10.1016/j.marpolbul.2023.115606.

[3] T. L. Yip, Port traffic risks–A study of accidents in Hong Kong waters, *Transportation Research Part E: Logistics and Transportation Review*, 2008, **44**, 921-931, doi: 10.1016/j.tre.2006.09.002.

[4] J. Wang, Y. Zhou, L. Zhuang, L. Shi, S. Zhang, Study on the critical factors and hot spots of crude oil tanker accidents, *Ocean & Coastal Management*, 2022, **217**, 106010, doi: 10.1016/j.ocecoaman.2021.106010.

[5] IACS C. Common structural rules for bulk carriers and oil tankers. International Association of Classification Societies. 2014.

[6] M. C. Xu, C. G. Soares, Comparisons of calculations with experiments on the ultimate strength of wide stiffened panels, *Marine Structures*, 2013, **31**, 82-101, doi: 10.1016/j.marstruc.2013.01.003.

[7] D. K. Kim, H. L. Lim, S. Y. Yu, A Technical review on ultimate strength prediction of stiffened panels in axial compression, *Ocean Engineering*, 2018, **170**, 392-406, doi: 10.1016/j.oceaneng.2018.10.022.

[8] D. K. Kim, S. Li, K. Yoo, K. Danasakaran, N.-K. Cho, An empirical formula to assess ultimate strength of initially deflected plate: part 2 = combined longitudinal compression and lateral pressure, *Ocean Engineering*, 2022, **252**, 111112, doi: 10.1016/j.oceaneng.2022.111112.

[9] H. Ma, D. Wang, Lateral pressure effect on the ultimate strength of the stiffened plate subjected to combined loads, *Ocean Engineering*, 2021, **239**, 109926, doi: 10.1016/j.oceaneng.2021.109926.

[10] G.-J. Shi, D.-W. Gao, H. Zhou, Analysis of hull girder ultimate strength and residual strength based on IACS CSR-H, *Mathematical Problems in Engineering*, 2019, **2019**, 2098492, doi: 10.1155/2019/2098492.

[11] L. Jiang, S. Zhang, Effect of pressure on collapse behaviour of stiffened panel, InMaritime Technology and Engineering, 2021.

[12] L. Jiang, S. Zhang, Lateral pressure effects on the ultimate strength of plates, Proceedings of ASME 2014 33rd International Conference on Ocean, Offshore and Arctic Engineering, 2015.

[13] M. C. Xu, Z. J. Song, J. Pan, C. G. Soares, Ultimate strength assessment of continuous stiffened panels under combined longitudinal compressive load and lateral pressure, *Ocean Engineering*, 2017, **139**, 39-53, doi: 10.1016/j.oceaneng.2017.04.042.

[14] J. Pan, N. Li, Z. J. Song, M. C. Xu, Influence of boundary condition and stiffener type on collapse behaviours of stiffened panels under longitudinal compression, *Advances in Mechanical Engineering*, 2019, **11**, 168781401988476, doi: 10.1177/1687814019884762.

[15] S. Sultana, Y. Wang, A. J. Sobey, J. A. Wharton, R. A. Shenoi, Influence of corrosion on the ultimate compressive strength of steel plates and stiffened panels, *Thin-Walled Structures*, 2015, **96**, 95-104, doi: 10.1016/j.tws.2015.08.006.

[16] D. K. Kim, H. L. Lim, M. S. Kim, O. J. Hwang, K. S. Park, An empirical formulation for predicting the ultimate strength of stiffened panels subjected to longitudinal compression, *Ocean Engineering*, 2017, **140**, 270-280, doi: 10.1016/j.oceaneng.2017.05.031.

[17] J. Parunov, C. Guedes Soares, Effects of Common Structural Rules on hull-girder reliability of an Aframax oil tanker, *Reliability Engineering & System Safety*, 2008, **93**, 1317-1327, doi: 10.1016/j.ress.2007.07.011.

[18] S. Tanaka, D. Yanagihara, A. Yasuoka, M. Harada, S. Okazawa, M. Fujikubo, T. Yao, Evaluation of ultimate strength of stiffened panels under longitudinal thrust, *Marine Structures*, 2014, **36**, 21-50, doi: 10.1016/j.marstruc.2013.11.002.

[19] A. AbuBakar, R. S. Dow, Simulation of ship grounding damage using the finite element method, *International Journal of Solids and Structures*, 2013, **50**, 623-636, doi: 10.1016/j.ijsolstr.2012.10.016.

[20] S. Li, A. Coraddu, L.Oneto, Computationally aware estimation of ultimate strength reduction of stiffened panels caused by welding residual stress: From finite element to data-driven methods, *Engineering Structures*, 2022, **264**, 114423, doi: 10.1016/j.engstruct.2022.114423.

[21] C. D. Jang, S. Y. Hong, Proceedings of the 17th International Ship and Offshore Structures Congress, Seoul: Seoul National University. 2009.

[22] W. Fricke, R. Bronsart, International ship and offshore structures congress (ISSC) 2012 in rostock/germany, *Ships*

and Offshore Structures, 2012, **7**, 351-355, doi: 10.1080/17445302.2012.743219.
[23] T. Yao, M. Fujikubo, Buckling and ultimate strength of ship and ship-like floating structures, Oxford: Butterworth-Heinemann. 2016.
[24] D. K. Kim, H. L. Lim, S. Y. Yu, A technical review on ultimate strength prediction of stiffened panels in axial compression, *Ocean Engineering*, 2018, **170**, 392-406, doi: 10.1016/j.oceaneng.2018.10.022.
[25] E. Tunca, B. Uğurlu, Ultimate strength analysis for the assessment of stiffener-plate design configuration, *Proceedings of TEAM*, 2015, 12-15, doi: 10.13140/RG.2.1.3393.1602.
[26] G. J. Shi, D. Y. Wang, B. Hu, S. J. Cai, Effect of initial geometric imperfections on dynamic ultimate strength of stiffened plate under axial compression for ship structures, *Ocean Engineering*, 2022, **256**, 111448, doi: 10.1016/j.oceaneng.2022.111448.
[27] C. Li, H. Ren, Z. Zhu, C G. Soares, Numerical investigation on the ultimate strength of aluminium integrally stiffened panels subjected to uniaxial compressive load, *Thin-Walled Structures*, 2018, **127**, 221-234, doi: 10.1016/j.tws.2018.01.003.
[28] S. F. Estefen, J. H. Chujutalli, C. Guedes Soares, Influence of geometric imperfections on the ultimate strength of the double bottom of a Suezmax tanker, *Engineering Structures*, 2016, **127**, 287-303, doi: 10.1016/j.engstruct.2016.08.036.
[29] B. Yang, J.-M. Wu, C. Guedes Soares, D.-Y. Wang, Dynamic ultimate strength of outer bottom stiffened plates under in-plane compression and lateral pressure, *Ocean Engineering*, 2018, **157**, 44-53, doi: 10.1016/j.oceaneng.2018.03.051.
[30] R. Adiputra, T. Yoshikawa, E. Erwandi, Reliability-based assessment of ship hull girder ultimate strength, *Curved and Layered Structures*, 2023, **10**, 20220189, doi: 10.1515/cls-2022-0189.
[31] A. E. Mansour, R. C. Ertekin, Proceedings of the 15th International Ship and Offshore Structures Congress, Amsterdam: Elsevier Science. 2003.
[32] Q. T. Do, T. Ghanbari-Ghazijahani, A. R. Prabowo, Developing empirical formulations to predict residual strength and damages in tension-leg platform hulls after a collision, *Ocean Engineering*, 2023, **286**, 115668, doi: 10.1016/j.oceaneng.2023.115668.
[33] Y. M. Lutfi, R. Adiputra, A. R. Prabowo, T. Utsunomiya, E. Erwandi, N. Muhayat, Assessment of the stiffened panel performance in the OTEC seawater tank design: Parametric study and sensitivity analysis, *Theoretical and Applied Mechanics Letters*, 2023, **13**, 100452, doi: 10.1016/j.taml.2023.100452.
[34] A. Nurcholis, A. R. Prabowo, I. Yaningsih, T. Muttaqie, H. Nubli, N. Huda, A. Fajri, Idealized fire-structures interaction on ship and offshore building members: a benchmark study using explicit-dynamic FE approach, *Procedia Structural Integrity*, 2023, **48**, 33-40, doi: 10.1016/j.prostr.2023.07.107.
[35] P. W. Adie, R. Adiputra, A. R. Prabowo, E. Erwandi, T. Muttaqie, N. Muhayat, N. Huda, Assessment of the OTEC cold water pipe design under bending loading: a benchmarking and parametric study using finite element approach, *Journal of the Mechanical Behavior of Materials*, 2023, **32**, 20220298, doi: 10.1515/jmbm-2022-0298.
[36] A. A. Pratama, A. R. Prabowo, T. Muttaqie, N. Muhayat, R. Ridwan, B. Cao, F. B. Laksono, Hollow tube structures subjected to compressive loading: implementation of the pitting corrosion effect in nonlinear FE analysis, *Journal of the Brazilian Society of Mechanical Sciences and Engineering*, 2023, **45**, 143, doi: 10.1007/s40430-023-04067-3.
[37] R. Ridwan, S. Sudarno, H. Nubli, A. Chasan, I. Istanto, P. S. Pratama, Numerical analysis of openings in stiffeners under impact loading: investigating structural response and failure behavior, *Mekanika: Majalah Ilmiah Mekanika*, 2023, **22**, 115-125, doi: 10.20961/mekanika.v22i2.76774.
[38] Y. M. Lutfi, R. Adiputra, A. R. Prabowo, N. Muhayat, H. Carvalho, T. Fazeres-Ferradosa, Ultimate strength value of stiffened panel designs under initial displacement and applied pressure: FE analysis *vs*. IACS-CSR, *Procedia Structural Integrity*, 2023, **47**, 660-667, doi: 10.1016/j.prostr.2023.07.055.
[39] M. I. Hanif, R. Adiputra, A. R. Prabowo, Y. Yamada, N. Firdaus, Assessment of the ultimate strength of stiffened panels of ships considering uncertainties in geometrical aspects: finite element approach and simplified formula, *Ocean Engineering*, 2023, **286**, 115522, doi: 10.1016/j.oceaneng.2023.115522.
[40] I. Faqih, R. Adiputra, A. R. Prabowo, N. Muhayat, S. Ehlers, M. Braun, Hull girder ultimate strength of bulk carrier (HGUS-BC) evaluation: structural performances subjected to true inclination conditions of stiffened panel members, *Results in Engineering*, 2023, **18**, 101076, doi: 10.1016/j.rineng.2023.101076.
[41] K. P. Jeom, Ultimate limit state performance of oil tanker structures designed by IACS common structural rules, *Thin-Walled Structures*, 2007, **45**, 1022-1034, doi: 10.1016/j.tws.2007.07.002.